J. Fluid Mech. (1982), *vol.* 123, *pp.* 31–41
Printed in Great Britain

Rising bubbles

By MICHAEL J. MIKSIS, JEAN-MARC VANDEN-BROECK
Department of Mathematics, Stanford University, California 94305

AND JOSEPH B. KELLER
Departments of Mathematics and Mechanical Engineering. Stanford University, California 94305

(Received 23 February 1981 and in revised form 19 April 1982)

The shape of a rising bubble, or of a falling drop, in an incompressible viscous fluid is computed numerically, omitting the condition on the tangential traction at the bubble or drop surface. When the bubble is sufficiently distorted, its top is found to be spherical and its bottom is found to be rather flat. Then the radius of its upper surface is in fair agreement with the formula of Davis & Taylor (1950). This distortion occurs when the effect of gravity is large while that of surface tension is small. When the effect of surface tension is large, the bubble is nearly a sphere.

The shape is found, together with the flow of the surrounding fluid, by assuming that both are steady and axially symmetric, with the Reynolds number being large. The flow is taken to be a potential flow. The boundary condition on the normal component of normal stress, including the viscous stress, is satisfied, but not that on the tangential component. The problem is converted into an integro-differential set of equations, reduced to a set of algebraic equations by a difference method, and solved by Newton's method together with parameter variation.

1. Introduction

When a bubble rises or a drop falls through a fluid, it is deformed from a spherical shape by the flow of the fluid around it and by the hydrostatic pressure due to gravity. Experiments show that small bubbles and drops are nearly spherical, but large ones are nearly spherical caps with rather spherical upper surfaces and concave lower surfaces (Davies & Taylor 1950). We wish to calculate the shapes of such deformed bubbles and drops, both of which we shall refer to as bubbles.

In order to calculate the shape we must simultaneously determine the flow of the surrounding fluid, treating the bubble surface as a free boundary. We want the problem to be steady, but since a bubble expands as it rises, its surface is not steady. To make it so, we assume that the bubble remains at a fixed height, with the surrounding fluid moving downward past it, both being axially symmetric. We also assume that the Reynolds number of the flow is large, so that the effects of viscosity are confined to a thin boundary layer around the bubble. Then by treating the surrounding fluid as incompressible, we can represent its motion as a potential flow, which automatically satisfies the Navier–Stokes equations.

One way to complete the formulation is to match this potential flow to the flow in the boundary layer. We shall not do this, because, even for a spherical bubble, the flow in the boundary layer is not known near the rear stagnation point on the axis of symmetry at colatitude $\theta = \pi$. The pressure drop $p_{\mathrm{BL}}(\theta)$ across the boundary

layer is known over the rest of the surface of the sphere (Moore 1963), but the expression for it has a non-integrable singularity at $\theta = \pi$.

As an alternative we ignore the boundary layer and use the potential flow right up to the boundary. This yields an exact solution of the Navier–Stokes equations throughout the fluid, with vanishing normal velocity on the surface of the bubble. We adjust this flow to make the normal component of normal stress vanish on the surface, but we cannot make the tangential component vanish. Because of this, the solution of this problem must be viewed as an approximation to that of the actual problem rather than as its high-Reynolds-number asymptotic form.

The major error introduced by ignoring the boundary layer is that due to neglecting the pressure drop $p_{\mathrm{BL}}(\theta)$ across it. Therefore we shall compare p_{BL} with the normal component of normal viscous stress σ_{rr}, which we do take into account. For a sphere, $p_{\mathrm{BL}}(\theta)$ is obtained by setting $y = 0$ in equation (2.37) of Moore (1963). Upon evaluating the integral in that equation we get

$$p_{\mathrm{BL}}(\theta) = \frac{12\rho U^2}{R} \frac{1}{\sin^3\theta} (\tfrac{2}{3} - \cos\theta + \tfrac{1}{3}\cos^2\theta). \tag{1.1}$$

Here R is the Reynolds number of the incident flow, which has velocity U at infinity, and ρ is the fluid density. On the other hand by computing σ_{rr} from the potential flow around a sphere we get

$$\sigma_{rr}(\theta) = 2\mu \frac{\partial}{\partial r}\left[-U\cos\theta\left(1 - \frac{a^3}{r^3}\right)\right]_{r=a} = \frac{12\rho U^2}{R}\cos\theta. \tag{1.2}$$

Here μ is the viscosity of the fluid and a is the radius of the bubble.

From these equations $p_{\mathrm{BL}}(\theta)/\sigma_{rr}(\theta) = 0$ at 0°, 0·045 at 10°, 0·095 at 20°, 0·16 at 30°, 0·31 at 45°, and 0·77 at 60°. We see that $p_{\mathrm{BL}} \leqslant 0{\cdot}31\ \sigma_{rr}$ from $\theta = 0$ to $\theta = 45°$. Davies & Taylor (1950) have shown that highly deformed bubbles have nearly spherical upper surfaces out to a rim at about 46° to 64°, so p_{BL} is less than one third of σ_{rr} over most of the upper surfaces of such bubbles. That the results for a sphere apply on the upper surface of such deformed bubbles has been shown by Bahga & Weber (1981), who found that the velocity measured in the boundary layer is nearly that given by potential theory, and it is even closer to that obtained by including Moore's boundary-layer correction.

On the lower surface p_{BL} is larger than on the upper surface and therefore it is not negligible. Furthermore the lower surface of a highly deformed bubble is adjacent to a turbulent wake, which we have not taken into account. Therefore we cannot expect the shape of the lower surface to be correct.

In addition to distorting the bubble, gravity exerts a buoyancy force $-F$ on it. A steady bubble is possible only if the flow exerts on it an opposite drag force F, and this force is supplied by the viscous stress. This is why we included this stress, even though our primary interest is in the effect of gravity. However our calculation does not take account of the turbulent flow in the wake of a highly distorted bubble, nor the pressure drop across the boundary layer, so it cannot yield the experimentally observed drag. In §5 we improve our calculation of the drag by the method of Levich (1949). This correction is important for nearly spherical bubbles. However, for highly distorted ones, where the effects of the turbulent wake dominate, the drag is still inaccurate.

Our formulation leads to a free-boundary problem for the bubble surface and the potential flow around it. It differs from similar problems that we solved previously

(Vanden-Broeck & Keller 1980; Miksis, Vanden-Broeck & Keller 1981) because it includes gravity and viscosity terms in the pressure boundary conditions. Nevertheless, we solve it by a similar method, which involves reduction to an integro-differential system of equations for the bubble surface and the potential on it. We discretize this system to convert it into a set of nonlinear algebraic equations. Then we solve these equations by Newton's method combined with parameter variation to provide the starting values. These steps are described in §§3 and 4, following the formulation in §2. Some of the results are shown in the figures, and they are discussed in §6.

2. Formulation

Let us consider an axially symmetric bubble of density ρ_b and pressure p_b at rest in an incompressible viscous fluid of density ρ and kinematic viscosity ν. We assume that the fluid is in steady motion past the bubble, and that at infinity it has velocity U along the z-axis. The Reynolds number of the flow is supposed to be high, and the flow is assumed to have a potential $\phi(r, z)$ outside a boundary layer around the bubble surface S. We suppose that the potential can be extended up to S, so that it satisfies the equations

$$\Delta\phi = 0 \quad \text{outside} \quad S, \tag{2.1}$$

$$\phi \sim Uz \quad \text{at infinity}, \tag{2.2}$$

$$\partial\phi/\partial n = 0 \quad \text{on} \quad S. \tag{2.3}$$

On S the balance of the normal component of normal stress is expressed by

$$-p + 2\rho\nu\frac{\partial u}{\partial n} = \sigma\kappa - p_b - \rho_b g z.$$

Here $\partial u/\partial n$ is the normal derivative of the normal velocity on S, κ is the mean curvature of S, σ is the surface tension, and p is the pressure in the fluid at S. We shall approximate p by the pressure just outside the boundary layer, which can be found from the Bernoulli equation

$$\tfrac{1}{2}(\nabla\phi)^2 - gz + \frac{p}{\rho} = \tfrac{1}{2}U^2 + \frac{p_\infty}{\rho} \quad \text{on} \quad S.$$

Here p_∞ is the pressure at infinity at $z = 0$ and g is the acceleration due to gravity. Upon eliminating p from the last two equations we obtain

$$\tfrac{1}{2}(\nabla\phi)^2 - \left(1 - \frac{\rho_b}{\rho}\right) gz - \frac{\sigma\kappa}{\rho} + \frac{2\nu\partial^2\phi}{\partial n^2} = \tfrac{1}{2}U^2 + \frac{p_\infty}{\rho} - \frac{p_b}{\rho} \quad \text{on} \quad S. \tag{2.4}$$

Now (2.1)–(2.4) constitute a problem for the determination of ϕ, S and some of the constants in (2.4).

It is convenient to introduce dimensionless variables into this problem by using U as the unit of velocity and r_e, the equivalent radius of the bubble, as the unit of length. This radius is defined by writing the volume V of the bubble as $\frac{4}{3}\pi r_e^3$. Thus in dimensionless variables

$$V = \tfrac{4}{3}\pi, \tag{2.5}$$

while (2.1)–(2.3) are unchanged except that U is replaced by unity in (2.2). However, (2.4) becomes

$$(\nabla\phi)^2 - \tfrac{3}{4}C_D z - \frac{4\kappa}{W} + 8R^{-1}\frac{\partial^2\phi}{\partial n^2} + \gamma = 0 \quad \text{on} \quad S. \tag{2.6}$$

In (2.6) we have introduced the following four dimensionless numbers:

$$\left.\begin{aligned} R &= \frac{2Ur_e}{\nu}, \qquad C_D = 8\left(1-\frac{\rho_b}{\rho}\right)\frac{gr_e}{3U^2}, \\ W &= \frac{2U^2r_e\rho}{\sigma}, \qquad \gamma = \frac{p_b-p_\infty-\frac{1}{2}\rho U^2}{\frac{1}{2}\rho U^2}. \end{aligned}\right\} \tag{2.7}$$

Here R is the Reynolds number, C_D is the drag coefficient, W is the Weber number and γ is the cavitation number.

In view of the axial symmetry of the bubble, we write the equation of its surface as $z = f_1(r)$ on the upstream face where $z < 0$, and as $z = f_2(r)$ on the downstream face where $z > 0$. Thus we choose the origin $z = 0$ to correspond to the maximum radius r_M at which $\dot{f}_1(r_M) = \infty$ and $\dot{f}_2(r_M) = \infty$. Then

$$f_1(r_M) = 0, \quad f_2(r_M) = 0, \tag{2.8}$$

and from symmetry, we must have on the z-axis

$$\dot{f}_1(0) = 0, \quad \dot{f}_2(0) = 0. \tag{2.9}$$

Another consequence of the symmetry is the occurrence of stagnation points at the two points where S intersects the z-axis. In terms of the tangential derivative $\partial/\partial s$ along S, this leads to the two conditions

$$\frac{\partial\phi[r, f_1(r)]}{\partial s} = 0, \quad \frac{\partial\phi[r, f_2(r)]}{\partial s} = 0 \quad \text{at} \quad r = 0. \tag{2.10}$$

The set of equations (2.1)–(2.3), (2.5), (2.6) and (2.8)–(2.10) constitute the problem for the determination of $\phi(r, z)$, $f_1(r)$ and $f_2(r)$. It is necessary to specify two of the four dimensionless parameters in (2.7) and then the other two must be found as part of the solution. In the absence of gravity and viscosity, (2.7) shows that $C_D = 0$ and $R = \infty$, so the problem reduces to that treated previously by Miksis *et al.* (1981). Then one of the remaining parameters γ and W had to be specified and the other had to be found.

3. Reformulation as an integro-differential system

We can simplify the problem just formulated by expressing the solution ϕ of (2.1)–(2.3) in terms of its values on S. To do so we introduce the axially symmetric Green function of (2.1), and apply Green's theorem to it and the function $\phi - z$. This function vanishes at infinity, in view of (2.2) with $U = 1$, and its normal derivative on S is just $-\partial z/\partial n$ because of (2.3). Finally we evaluate the resulting expression for $\phi - z$ on the surface S. This derivation is the same as that in Miksis *et al.* (1981). In this way we obtain the following integral equation for the value of ϕ on S, in which the functions f_1, f_2 and their first derivatives occur:

$$\begin{aligned} 2\pi[\phi[r, f_i(r)] - f_i(r)] = &\int_0^{r_M} sds\left[\{\phi[s, f_2(s)] - f_2(s)\}\left\{-\dot{f}_2(s)\frac{\partial g_2}{\partial s} + \frac{\partial g_2}{\partial f_2}\right\} + g_2\right] \\ &- \int_0^{r_M} sds\left[\{\phi[s, f_1(s)] - f_1(s)\}\left\{-\dot{f}_1(s)\frac{\partial g_1}{\partial s} + \frac{\partial g_1}{\partial f_1}\right\} + g_1\right] \quad (i = 1, 2). \end{aligned} \tag{3.1}$$

Here we have introduced the notation

$$g_j = \frac{4}{(l_j^2+k^2)^{\frac{1}{2}}} K\left(\frac{k^2}{k^2+l_j^2}\right),$$
$$k^2 = 4rs,$$
$$l_j^2 = (s-r)^2+[f_i(r)-f_j(s)]^2,$$

with $K(m)$ the complete elliptic integral of the first kind.

The problem is now that of solving (3.1), (2.5), (2.6) and (2.8)–(2.10) for $f_1(r), f_2(r)$, the value of ϕ on S, and two of the four parameters in (2.7).

4. Numerical method

Before describing the numerical method, we replace r by the new independent variable t defined by

$$r = r_M(1-t^2) \quad (-1 \leqslant t \leqslant 1). \tag{4.1}$$

Then we replace f_1 and f_2 by the new dependent function $\beta(t)$ given by

$$\left.\begin{aligned} \beta(t) &= \frac{f_1[r(t)]}{r_M} \quad (-1 \leqslant t \leqslant 0), \\ \beta(t) &= \frac{f_2[r(t)]}{r_M} \quad (0 \leqslant t \leqslant 1). \end{aligned}\right\} \tag{4.2}$$

We also introduce $\xi(t)$ by

$$\xi(t) = \frac{\phi[r(t), r_M\,\beta(t)]}{r_M} \quad (-1 \leqslant t \leqslant 1). \tag{4.3}$$

The reason for introducing these changes is that the functions $f_1(r)$ and $f_2(r)$, and therefore $\phi[r, f_1(r)]$, are singular at r_M. The new functions $\beta(t)$ and $\xi(t)$ are regular at the corresponding point $t = 0$.

Now for some integer N, we introduce the mesh points t_I and $t_{I+\frac{1}{2}}$ defined by

$$t_I = \frac{I-1}{N-1} - 1 \quad (I = 1, \ldots, 2N-1), \tag{4.4}$$

$$t_{I+\frac{1}{2}} = \frac{I-\frac{1}{2}}{N-1} - 1 \quad (I = 1, \ldots, 2N-2). \tag{4.5}$$

We also introduce the corresponding quantities

$$\beta_I = \beta(t_I) \quad (I = 1, \ldots, 2N-1), \tag{4.6}$$

$$\xi_{I+\frac{1}{2}} = \xi(t_{I+\frac{1}{2}}) \quad (I = 1, \ldots, 2N-2). \tag{4.7}$$

We shall determine these quantities to satisfy (2.6) and (3.1) at the $2N-3$ mesh points t_I, $I = 2, \ldots, 2N-2$. To evaluate ξ at t_I we use linear interpolation between the values of ξ at $t_{I-\frac{1}{2}}$ and $t_{I+\frac{1}{2}}$.

The logarithmic singularities introduced by the Green functions are integrated by a method similar to that of Longuet-Higgins & Cokelet (1976), and the integrals are evaluated by the trapezoidal rule. The derivative $\partial^2\phi/\partial n^2$ is expressed in terms of the tangential derivative $\partial^2\phi/\partial s^2$ with the aid of Laplace's equation. The procedure follows that of Vanden-Broeck & Keller (1980) and Miksis (1981), where more details are given.

The foregoing procedure yields $4N-6$ nonlinear algebraic equations involving the $4N+2$ quantities β_I, $\xi_{I+\frac{1}{2}}$, R, C_D, W, γ and r_M. We obtain two more equations from (2.9) by using a three-point Lagrange difference formula and two equations from (2.10) by means of a three-point Lagrange extrapolation formula. Then (2.5) and (2.8) each gives one more equation for a total of $4N$ equations. Thus by specifying two of the parameters, for example γ and C_D, we have $4N$ unknowns and $4N$ equations.

We solve these equations by Newton's method, so we need values with which to start the iteration procedure. For given values of the specified parameters, we use as starting values the final or 'converged' solution for slightly different parameter values for which we have already solved the equations. Similarly, when we increase the value of N, we start with the solution for a slightly smaller value of N, augmented by interpolation and extrapolation.

To obtain an overall start, we use the fact that as γ tends to infinity, the bubble tends to a sphere of unit radius, for which ϕ can be found explicitly. We can also construct the asymptotic form of the solution for large γ by seeking it as an expansion in powers of γ^{-1}. By solving the equations of §2 with γ and R given, we find

$$r = 1 - \frac{9\cos^2\theta - 3}{8\gamma} + O(\gamma^{-2}), \tag{4.8}$$

$$W = 8\gamma^{-1} - 12\gamma^{-2} + O(\gamma^{-3}), \tag{4.9}$$

$$C_D = 32R^{-1} + O(\gamma^{-1}). \tag{4.10}$$

In these equations ρ and θ are polar coordinates in the (r, z)-plane, with θ measured from the z-axis. Thus (4.8) shows that the bubble is an oblate ellipsoid of revolution when terms of order γ^{-2} are negligible. Harper (1972, equation (2.45)) obtained (4.8) with γ replaced by $8/W$, which follows from (4.9), and Moore (1963) obtained (4.10).

5. Levĭch's method

Neglecting the pressure drop across the boundary layer has introduced some error into our calculations. The magnitude of this error was indicated by Moore (1963), who obtained the result (4.10), $C_D = 32R^{-1}$, for a spherical bubble, whereas the correct value obtained by Levich (1949) is $C_D = 48R^{-1}$. Our calculation of C_D for non-spherical bubbles must also be in error, so we shall correct it by adapting Levich's method. He has shown that for large Reynolds numbers the energy dissipation rate D of the flow can be found by using the potential flow in the integral for D. Then D can be transformed into the following form (Lamb 1932, p. 580):

$$D = \nu\rho \int_S \frac{\partial}{\partial n}(\nabla\phi)^2 \, dS. \tag{5.1}$$

Now D is also equal to the power UF delivered by the drag force F, which is the negative of the buoyancy force $-\frac{4}{3}\pi r_e^3(\rho - \rho_b)g$. Upon equating UF to D given by (5.1), and introducing the dimensionless variables defined in (2.7), we obtain

$$C_D = \frac{4I}{\pi R}. \tag{5.2}$$

Here the dimensionless integral I is defined by

$$I = \frac{1}{r_e U^2} \int_S \frac{\partial}{\partial n}(\nabla\phi)^2 \, dS. \tag{5.3}$$

Thus by using the potential flow in (5.3), we can obtain an improved value for C_D from (5.2), or if C_D is given we get an improved value for R.

6. Discussion of results

In discussing bubbles it is customary to introduce the Morton number

$$M = g\left(1-\frac{\rho_b}{\rho}\right)\frac{\rho^3\nu^4}{\sigma^3}, \tag{6.1}$$

which depends upon physical properties of the fluid, but not upon the size or velocity of the bubble. The other dimensionless parameters are related to M by the identity

$$M = \frac{3C_D W^3}{4R^4}. \tag{6.2}$$

Therefore we can specify two parameters, say γ and C_D, solve for the flow, the bubble shape, W and R, and then find M from (6.2). Alternatively, by using in (6.2) the improved value for R given by (5.2), we obtain instead

$$M = \frac{3\pi^4 C_D^5}{1024} W^3 I^{-4}. \tag{6.3}$$

When we wish to specify the values of M and γ, we adjoin (6.3) to the set of $4N$ equations, and we include the three parameters R, W and C_D as unknowns. Then we have a set of $4N+1$ equations for $4N+1$ unknowns.

We have used the numerical method of §4 to calculate bubble shapes for various parameter values. To illustrate the convergence of the method, we consider the case $\gamma = 0$ and $M = 1{\cdot}75\times10^{-7}$. For $N = 10$, 15 and 20, we found for W the values 3·3283, 3·3852 and 3·4052, respectively. For the axial ratio χ of the bubble, defined by $\chi = 2r_M[f_2(0)-f_1(0)]^{-1}$, we obtained 3·524, 3·553 and 3·563 respectively. These results indicate that the method converges.

As a further test of the method, we computed the solution for the large value $\gamma = 50$ with $M = 2{\cdot}6\times10^{-11}$ using $N = 15$, and compared the results with the asymptotic formulae (4.8) and (4.9). The numerical results were $\rho(0) = 0{\cdot}989$, $\rho(\frac{1}{2}\pi) = 1{\cdot}0085$ and $W = 0{\cdot}1551$. The corresponding asymptotic results were $\rho(0) = 0{\cdot}985$, $\rho(\frac{1}{2}\pi) = 1{\cdot}0075$ and $W = 0{\cdot}1552$. This agreement indicates that both results are correct for this value of γ.

Another confirmation of our results is their agreement for small M ($M < 10^{-10}$) with those we obtained in the absence of gravity and viscosity (Miksis *et al* 1981). Since M is zero when either $g = 0$ or $\nu = 0$, this agreement is to be expected.

Figure 1 shows two examples of computed bubble profiles for one value of M and two values of γ, while figure 2 shows two more examples for a larger value of M and the same two values of γ. As we expect, the bubbles with the smaller value of γ are more distorted than those with the larger value.

Davies & Taylor (1950) observed that the tops of large bubbles are very nearly spherical. They concluded that the flow around the top is approximately that around a sphere. By using this flow in the Bernoulli equation near the top, they derived a relation between the velocity of rise U and the radius of curvature r_c at the top. In our dimensionless variables it is

$$C_D = 6\left(1-\frac{\rho_b}{\rho}\right)\frac{1}{r_c}. \tag{6.4}$$

This relation fits the experimental data quite well.

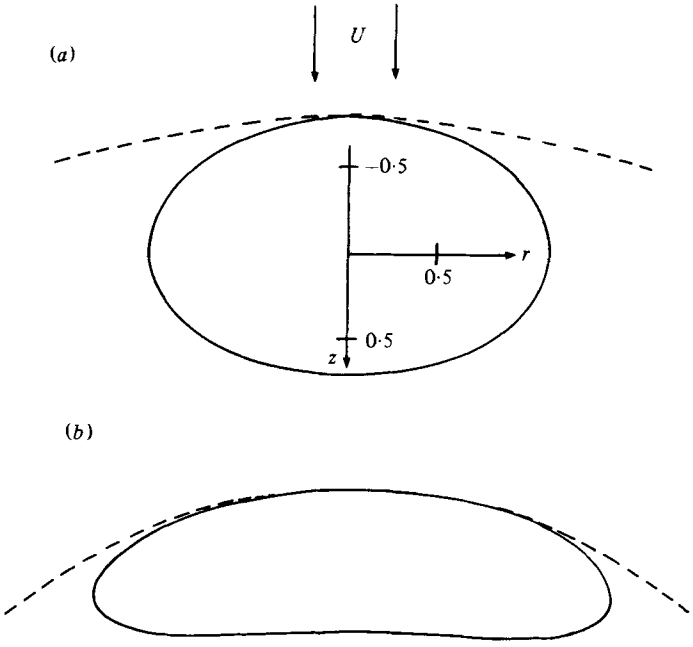

FIGURE 1. Computed bubble profiles for $M = 1{\cdot}75 \times 10^{-7}$ and (*a*) $\gamma = 2$, (*b*) $\gamma = 0$. Computed value of $C_D = 1{\cdot}07$ in (*a*) and $C_D = 2{\cdot}05$ in (*b*). Dashed curves are circular arcs with radii given by the Davies–Taylor formula (6.4). The unit of length is r_e.

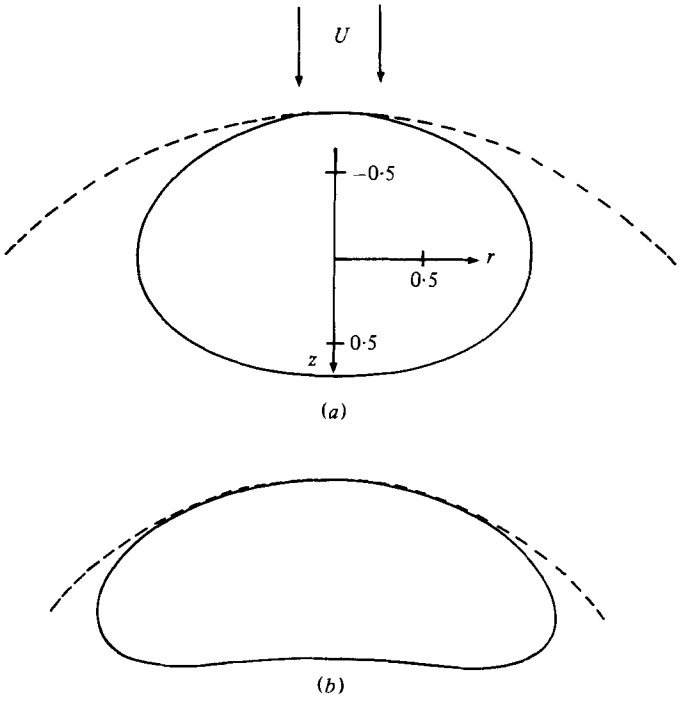

FIGURE 2. Same as figure 1 but for $M = 1{\cdot}0 \times 10^{-5}$. Computed value of $C_D = 2{\cdot}3$ in (*a*) and $C_D = 3{\cdot}0$ in (*b*).

We have compared (6.4) with the results of our computations. Such comparisons are shown in figures 1 and 2. In them each dotted line is an arc of a circle with the radius r_c determined by (6.4) from the value of C_D for the bubble shown. The figures show that the agreement is good for $\gamma = 0$ and for the two values of M. These values of M are both large, indicating that gravity and viscosity are important. However, in figure 2 the value of M is $1{\cdot}0 \times 10^{-5}$, whereas for water $M \approx 2{\cdot}6 \times 10^{-11}$. Thus to obtain bubbles that resemble those in water we must use a much larger value of M than that of water. This is a consequence of the fact, mentioned earlier, that our method ignores the turbulence that occurs in the wake of a real distorted bubble.

For γ fixed our computations suggest that there is a maximum value of M above which no solutions exist. For $\gamma = 0$ this value is approximately $M = 10^{-4}$.

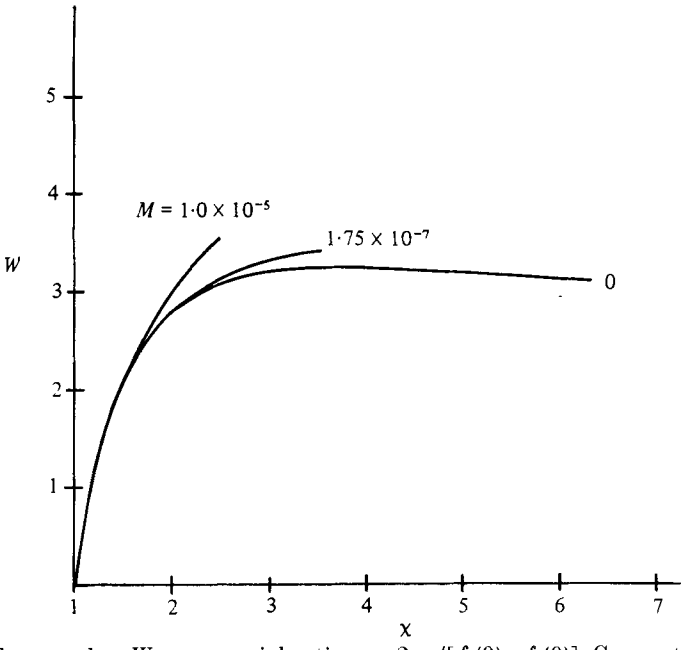

FIGURE 3. Weber number W versus axial ratio $\chi = 2r_M/[f_2(0) - f_1(0)]$. Curves terminated where $r = 0$.

In figure 3 we plot the Weber number W versus the axial ratio χ for three values of M. The cavitation number γ decreases along each curve until it becomes zero, at which point we terminated the curve. We see that as M increases, so does W, for fixed axial ratio. Otherwise the behaviour is similar to that in the inviscid case.

Figure 4 is a plot of $C_D M^{-\frac{1}{5}}$ verses $RM^{\frac{1}{5}}$. The inviscid results of Miksis (1981), corresponding to $M = 0$, are plotted along with the results for $M = 1{\cdot}25 \times 10^{-7}$ and $M = 1{\cdot}0 \times 10^{-5}$. Again we stop the calculation at $\gamma = 0$. The bottom curve is rather flat and horizontal near the point where $\gamma = 0$, indicating that C_D is rather independent of R there. Then the shape is determined mainly by C_D, as (6.4) indicates.

In figure 5 we plot the terminal velocity U as a function of r_e, the equivalent radius of the bubble, for three values of M. To obtain U and r_e we use (2.7) and then eliminate W by means of (6.2). In this way we get

$$\left.\begin{aligned} U\left[\nu g\left(1-\frac{\rho_b}{\rho}\right)\right]^{-\frac{1}{3}} &= \left(\frac{4R}{3C_D}\right)^{\frac{1}{3}}, \\ r_e\left[\left(1-\frac{\rho_b}{\rho}\right)\frac{\rho g}{\sigma}\right]^{\frac{1}{2}} &= \tfrac{1}{4}(3C_D W)^{\frac{1}{2}} = (\tfrac{3}{4}C_D)^{\frac{2}{3}}(R^4 M)^{\frac{1}{3}}. \end{aligned}\right\} \tag{6.5}$$

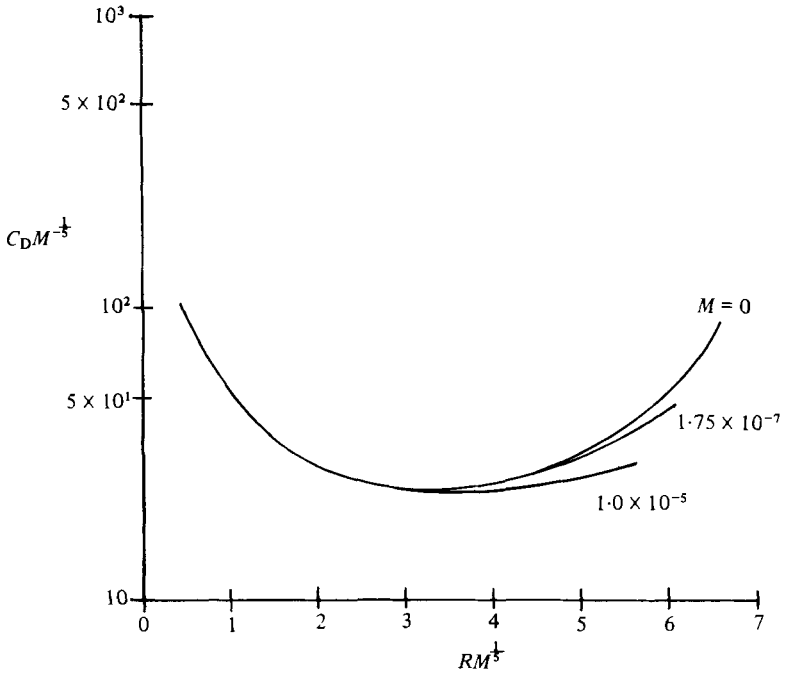

FIGURE 4. $C_D M^{-\frac{1}{3}}$ versus $RM^{\frac{1}{3}}$. The results for $M = 0$ are from Miksis *et al.* (1981). The curves were terminated where $r = 0$.

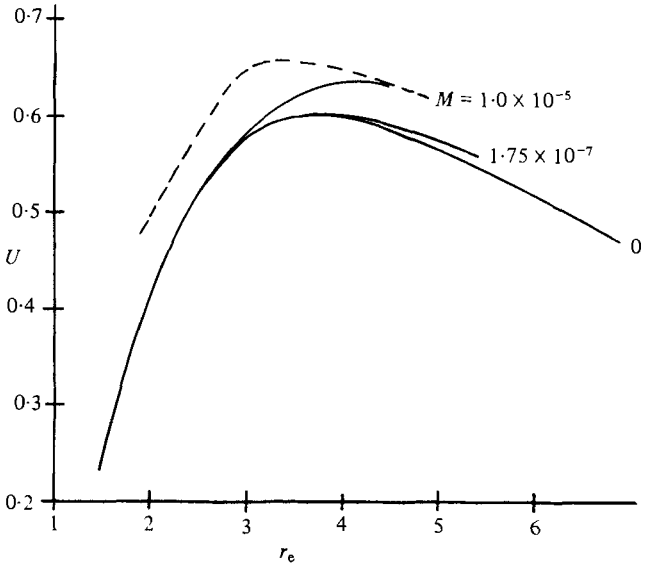

FIGURE 5. Terminal velocity U as a function of bubble equivalent radius r_e. The unit of U is $[\nu g(1-\rho_b/\rho)]^{\frac{1}{3}} M^{-\frac{2}{15}}$ and the unit of r_e is $[(1-\rho_b/\rho)\rho g/\sigma]^{-\frac{1}{2}} M^{\frac{1}{10}}$. The dashed line from figure 6 of Moore (1965) represents the experimental data of Haberman & Morton (1953) for air bubbles in Varsol with $M = 4{\cdot}45 \times 10^{-10}$, $\sigma = 24{\cdot}5$, $\rho = 0{\cdot}782$ and $\mu = 0{\cdot}0085$. These values yield 38·9 cm/s for the unit of U and 0·021 cm for the unit of r_e.

The computed values of C_D and R are used in (6.5) to find the values of U and r_e shown in figure 5. The dashed line in the figure is a smoothed curve drawn through the experimental points of Haberman & Morton (1953). The properties of the fluid, listed in the caption, are from the caption of figure 6 in Moore (1965). Since $M = 4{\cdot}45 \times 10^{-10}$, the experimental curve should be compared with the theoretical curve for $M = 0$, which is the smallest value of M shown in the figure. If a logarithmic scale were used for U, the agreement between theory and experiment would appear about the same as in Moore's figure 6.

This research was supported in part by the Army Research Office, the Office of Naval Research, the Air Force Office of Scientific Research and the National Science Foundation.

REFERENCES

BHAGA, D. & WEBER, M. E. 1981 *J. Fluid Mech.* **105**, 61–85.

DAVIES, R. M. & TAYLOR, G. I. 1950 *Proc. R. Soc. Lond.* A **200**, 375–390.

HABERMAN, W. L. & MORTON, R. K. 1953 Experimental investigation of the drag on air bubbles rising in various liquids. *Tech. Rep.* no. 802, *David Taylor Model Basin, Washington, D.C.*

HARPER, J. F. 1972 *Adv. Appl. Mech.* **12**, 59–129.

LAMB, H. 1932 *Hydrodynamics*, 6th edn. Cambridge University Press.

LEVICH, V. G. 1949 *Zh. Eksp. Teor. Fiz.* **19**, 18–24.

LONGUET-HIGGINS, M. S. & COKELET, E. D. 1976 *Proc. R. Soc. Lond.* A **350**, 1–26.

MIKSIS, M. 1981 Numerical solution of hydrodynamic free boundary problems. Ph.D. thesis, Courant Institute of Mathematical Sciences, New York University.

MIKSIS, M., VANDEN-BROECK, J.-M. & KELLER, J. B. 1981 *J. Fluid Mech.* **108**, 89–100.

MOORE, D. W. 1963 *J. Fluid Mech.* **16**, 161–176.

MOORE, D. W. 1965 *J. Fluid Mech.* **23**, 749–766.

VANDEN-BROECK, J.-M. & KELLER, J. B. 1980 *J. Fluid Mech.* **101**, 673–686.